⌘ *Author's Choice*

THE JOURNAL OF BIOLOGICAL CHEMISTRY VOL. 284, NO. 50, pp. 35227–35239, December 11, 2009

Functional Characterization of Intracellular *Dictyostelium discoideum* P2X Receptors*[S]

Received for publication, August 3, 2009, and in revised form, October 6, 2009 Published, JBC Papers in Press, October 15, 2009, DOI 10.1074/jbc.M109.045674

Melanie J. Ludlow, Latha Durai, and Steven J. Ennion[1]

From the Department of Cell Physiology and Pharmacology, University of Leicester, Leicester LE1 9HN, United Kingdom

Indicative of cell surface P2X ion channel activation, extracellular ATP evokes a rapid and transient calcium influx in the model eukaryote *Dictyostelium discoideum*. Five P2X-like proteins (dP2XA–E) are present in this organism. However, their roles in purinergic signaling are unclear, because dP2XA proved to have an intracellular localization on the contractile vacuole where it is thought to be required for osmoregulation. To determine functional properties of the remaining four dP2X-like proteins and to assess their cellular roles, we recorded membrane currents from expressed cloned receptors and generated a quintuple knock-out *Dictyostelium* strain devoid of dP2X receptors. ATP evoked inward currents at dP2XB and dP2XE receptors but not at dP2XC or dP2XD. β,γ-Imido-ATP was more potent than ATP at dP2XB but a weak partial agonist at dP2XE. Currents in dP2XB and dP2XE were strongly inhibited by Na^+ but insensitive to copper and the P2 receptor antagonists pyridoxal phosphate-6-azophenyl-2′,4′-disulfonic acid and suramin. Unusual for P2X channels, dP2XA and dP2XB were also Cl^--permeable. The extracellular purinergic response to ATP persisted in *p2xA/B/C/D/E* quintuple knock-out *Dictyostelium* demonstrating that dP2X channels are not responsible. dP2XB, -C, -D, and -E were found to be intracellularly localized to the contractile vacuole with the ligand binding domain facing the lumen. However, quintuple *p2xA/B/C/D/E* null cells were still capable of regulating cell volume in water demonstrating that, contrary to previous findings, dP2X receptors are not required for osmoregulation. Responses to the calmodulin antagonist calmidazolium, however, were reduced in *p2xA/B/C/D/E* null cells suggesting that dP2X receptors play a role in intracellular calcium signaling.

Purinergic signaling is one of the most primitive forms of eukaryotic cell communication with pharmacological evidence for its existence in plants, invertebrates, and vertebrates (1). Receptors that mediate responses to extracellular purines include both ligand gated ion channels (P2X receptors) and G-protein-coupled receptors (P2Y, adenosine and cAMP receptors). ATP is the exclusive endogenous ligand at mammalian P2X receptors, which consist of seven distinct subtypes ($P2X_{1-7}$) that assemble at the cell surface as homo- or heterotrimeric channels and play key roles in a wide range of physiological processes such as neurotransmission, platelet aggregation, smooth muscle contraction, and immune cell function (2, 3). Definitive molecular and functional evidence for P2X receptors has also been obtained in several lower organisms, including species of trematode (4), amoeba (5), green algae (6), choanoflagellate (6), and tardigrade (7), making it clear that the emergence of P2X receptors was an early event in eukaryotic evolution. What is less clear however is whether the physiological roles of these lower organism P2X receptors are analogous to the cell surface function of vertebrate P2X receptors.

The amoeba *Dictyostelium discoideum* has recently emerged as a potential model system for fundamental aspects of purinergic signaling due to the simplicity and genetic tractability of this organism, with the availability of powerful functional screens, and also due to the absence of P2X-like proteins in the genomes of other key model organisms such as yeast, *Caenorhabditis elegans*, and *Drosophila*. Sequencing of the *Dictyostelium* genome (8) revealed the presence of five genes with weak homology to vertebrate P2X receptors (named *p2xA*, *p2xB*, *p2xC*, *p2xD*, and *p2xE* in Dictybase (9)). Of these five genes *p2xA* shows the most homology to vertebrate P2X receptors and was shown to encode an ATP-gated ion channel when exogenously expressed in HEK293 cells (5). Interestingly, rather than being located on the plasma membrane analogous to vertebrate P2X receptors, the native dP2XA protein was found to be localized to the intracellular membranes of the contractile vacuole where it is thought to be required for osmoregulation (5), thus highlighting the possibility of potential novel intracellular roles for vertebrate P2X receptors.

In addition to the intracellular signaling mediated by dP2XA, *Dictyostelium* also possesses a purinergic signaling system for extracellular nucleotides more analogous to that found in vertebrate cells. Using an apoaequorin-expressing strain we have previously demonstrated that both extracellular ATP and ADP evoke a robust and rapid increase in intracellular Ca^{2+} in *Dictyostelium* (10). The characteristics of this purinergic response are indicative of the involvement of an ionotropic P2X rather than a metabotropic P2Y-like receptor, because it is dependent on extracellular Ca^{2+} and is unaffected by ablation of either the G-protein subunit gene *Gβ* or the inositol 1,4,5-trisphosphate receptor gene *iplA* (10). However, there are notable differences compared with Ca^{2+} responses via vertebrate P2X receptors, including

* This work was supported by the Wellcome Trust (Project Grant WT081601MA).
⌘ *Author's Choice*—Final version full access.
[S] The on-line version of this article (available at http://www.jbc.org) contains supplemental Figs. S1 and S2.
[1] To whom correspondence should be addressed: Dept. of Cell Physiology and Pharmacology, Medical Sciences Bldg., University Road, University of Leicester, Leicester LE1 9HN, United Kingdom. Tel.: 0116-229-7134; Fax: 0116-252-5045; E-mail: se15@le.ac.uk.

equal sensitivity to both ATP and ADP and lack of effect of the common P2 receptor antagonists PPADS[2] and suramin. The exclusive involvement of either the *p2xA* or *p2xE* genes in the extracellular purinergic response was ruled out by ablation of these genes (10), leaving, *p2xB*, *p2xC*, and *p2xD* as the most likely candidate receptors.

In this study we aimed to determine whether the other four members of the *Dictyostelium* P2X receptor family also correspond to ATP-gated ion channels and to assess the roles of dP2X receptors in purinergic signaling by generating a quintuple knock-out strain with all five *p2x* genes ablated. We show that dP2XB and dP2XE do correspond to ATP-gated channels but could not obtain functional currents for dP2XC or dP2XD receptors. Apart from a decrease in magnitude, the extracellular purinergic response remained unaffected in quintuple *p2x* knock-out *Dictyostelium*, demonstrating that the cell surface ATP/ADP receptor is not a P2X channel. Indeed all five dP2X proteins proved to be intracellular, localized to the contractile vacuole membrane with the ligand binding domain facing the lumen. When exposed to distilled water, quintuple *p2x* null cells displayed a slight delay in their osmoregulatory response but, in marked contrast to previous studies with *p2xA* null cells (5), were still capable of regulating their cell volume demonstrating a minor and nonessential role for dP2X receptors in osmoregulation. Calcium responses to both calmidazolium and ATP, however, were reduced in quintuple *p2x* null cells suggesting that dP2X receptors play a role in intracellular calcium signaling.

EXPERIMENTAL PROCEDURES

Cloning of Dictyostelium P2X Receptors—Oligonucleotide primers (pairs 1–5, see Table 1) designed to amplify the coding regions of the five predicted *Dictyostelium* P2X receptor genes (DDB0238349, DDB0238356, DDB0238363, DDB0238366, and DDB0238352 for *p2xA–E*, respectively) were utilized for reverse transcription-PCR on cDNA prepared from Ax2 *Dictyostelium*. First strand cDNA was used directly as template in PCR reactions containing 200 μM dNTP, 1.5 mM $MgCl_2$, 25 pmol of each primer, 1× Opti-Buffer (Bioline, UK), and 2.5 units of Bio-X-Act *Taq* DNA polymerase (Bioline). Thermal cycling consisted of 30 repetitions of 94 °C for 30 s, 56 °C for 1 min, and 72 °C for 1.5 min. PCR products were cloned into pcDNA3.1 (Invitrogen), and independent clones were sequenced on both strands.

Electrophysiological Recordings—Sense strand cRNA was generated from MluI-digested dP2X plasmids with a T7 mMessage mMachine™ kit (Ambion, Austin, TX). Manually defolliculated stage V *Xenopus* oocytes were injected with 50 ng of cRNA and stored at 18 °C in ND96 buffer (96 mM NaCl, 2 mM KCl, 1.8 mM $CaCl_2$, 1 mM $MgCl_2$, 5 mM sodium pyruvate, 5 mM HEPES, pH 7.6) prior to recording 3–7 days later. Two-electrode voltage clamp recordings were made from dP2X-expressing *Xenopus* oocytes at room temperature using an Axoclamp 900A amplifier with a Digidata 1440A data acquisition system and pClamp 10 acquisition software (Molecular Devices). For construction of concentration response data, the extracellular recording solution (ND98K^+) consisted of 98 mM KCl, 1.8 mM $BaCl_2$, 1 mM $MgCl_2$, 5 mM MES, pH 6.2. Membrane currents were recorded at a holding potential of −70 mV. ATP (Mg^{2+} salt, Sigma) was applied from a nearby U-tube perfusion system, whereas antagonists (PPADS and suramin (Sigma)), $CuCl_2$, and ivermectin (Sigma) were bath perfused as well as being present at the appropriate concentration in the U-tube application of ATP. For dP2XE reproducible currents were obtained with a 5-min recovery period between sequential applications of agonist allowing concentration response data to be obtained sequentially in individual cells. Marked current rundown, however, occurred with dP2XA and dP2XB, which was highly dependent on the previous history of ATP applications. This prevented construction of concentration response data in the same cells, and, to overcome this, a single application of agonist was made to 10–15 oocytes from the same batch for each concentration of agonist, and a mean peak response was taken. Non-injected and water-injected oocytes tested from at least five batches of oocytes gave no detectable currents in response to ATP or ADP application (tested at 3 mM). Concentration response data were fitted using GraphPad Prism 5.0 software (San Diego, CA).

For permeability ratio studies the external recording solution consisted of: either NaCl, KCl, NH_4Cl, or choline chloride at 98 mM, 1.8 mM $BaCl_2$, 1 mM $MgCl_2$, and 5 mM MES (pH 6.2). Reversal potentials (V_{rev}) for currents in different test cation solutions were obtained using a dual ramp protocol, which stepped from a holding potential of −70 mV to +70 mV for 0.2 s followed by a ramp down to −100 mV over 1.6 s and a ramp up to +70 mV over 1.6 s before a step back to −70 mV. This voltage protocol was first applied in the absence of ATP to control for endogenous voltage-activated currents, and then in the presence of ATP (3 mM) the two traces were superimposed. The reversal potential was taken as the points where the current traces crossed on the ramps (Fig. 4*A*). The difference between the two cross-over points obtained for each cell (up-ramp and down-ramp) was typically <2 mV, and the mean of the two values was taken as the reversal potential for each cell ($n \geq 6$ cells). Relative permeability ratios for monovalent cations were calculated using Equation 1,

$$P_X/P_{Na} = \exp(\Delta V_{rev} F/RT) \quad \text{(Eq. 1)}$$

where F is Faraday's constant, R is the universal gas constant, and T is the absolute temperature.

Chloride permeability measurements were made in external solutions where KCl was substituted with potassium gluconate so as to keep [K^+] constant while lowering [Cl^-]. Gluconate has previously been show to be impermeable to human $P2X_5$ channels (11). Solutions consisted of 1.8 mM $BaCl_2$, 1 mM $MgCl_2$, 5 mM MES, and either 9.8 mM KCl plus 88.2 mM potassium gluconate, 49 mM KCl plus 49 mM potassium gluconate, or 98 mM KCl (pH 6.2). ATP was applied at 3 mM, and the reversal potential at different Cl^- concentrations was determined with the

[2] The abbreviations used are: PPADS, pyridoxal phosphate-6-azophenyl-2′,4′-disulfonic acid; MES, 4-morpholineethanesulfonic acid; GFP, green fluorescent protein; RFP, red fluorescent protein; bsr, blasticidin S resistance cassette; MOPS, 4-morpholinepropanesulfonic acid; eGFP, enhanced GFP; PBS, phosphate-buffered saline; TBS, Tris-buffered saline.

TABLE 1

Oligonucleotide primers

Primer pairs 1–5 = cDNA amplification (the first 9 bases in the forward primers correspond to a mammalian Kozak sequence), 6–10 = dP2X-eGFP/RFP construct generation, and 11–16 = *p2x* disruption construct generation. Restriction endonuclease sites incorporated into primer sequences are in bold.

		Forward primer (5′-3′)	Reverse primer (5′-3′)
1	dP2XA	GCCGCCACCATGGGTTTTAGTTTTGATTGG	TTAAAAAAAAGTAGTAGTAGTAGTAATATTAC
2	dP2XB	GCCGCCACCATGACAATTGATTGGGACTC	AAAAATTTCTCCCATTTTATTGTTATTATTA
3	dP2XC	GCCGCCACCATGTTAGATTGGGATTCTATTCTAG	AAAAATTTATAAAACACAAGAATTATTTGG
4	dP2XD	GCCGCCACCATGGATTGGGATAATATTTTTTC	AATAATTATATTATTTACATTTTTATTTATTTATTTG
5	dP2XE	GCCGCCACCATGAATTTCAGAAATATTGATTGG	ACAATTTATTTTATTACCCGATTAATATATTTG
6	dP2XB	AAAA**AAGCTT**AAAAAATGACAATTGATTGGGACTC	AAAA**GGATCC**AATAGAGCTTCAATATTATGATAAAG
7	dP2XC	AAAA**AAGCTT**AAAAAATGTTAGATTGGGATTCTATTC	AAAA**GGATCC**AATAGAGCTTCAATGTTATGATAAAG
8	dP2XD	AGAG**AAGCTT**AAAAAATGGATTGGGATAATATTTTTTC	AGAG**GGATCC**AATAAAATTATATTATTATTTTTGAATATTTTG
9	dP2XE	AAAA**AAGCTT**AAAAAATGAATTTCAGAAATATTG	TTAA**GGATCC**AATTTCTCATAACTATTATTTTG
10	RFP	GGGG**GGATCC**ACCGGTCGCCACCATGGCATCATCAGAAGATG	CGCG**TCTAGA**TTATGCACCTGTTGAATGTCTACC
11	5′ *p2xB*	AAAA**GGGCCC**GAATTATGTGAAAACATTAATTTG	GATT**AAGCTT**CATCTGGAGCCAATAATGAAG
12	3′ *p2xB*	TATT**GCGGCCGC**GATAAACTTTATCATAATATTGAAG	AAAT**CCGCGG**TGAAATTACGCCTTGATGAC
13	5′ *p2xC*	TCGT**GGGCCC**TATATTTTAATAGTACCCTTTTACC	ACAT**AAGCTT**ATAGGCTAGAATAGAATCTTAAG
14	3′ *p2xC*	TGCA**GCGGCCGC**AATTTATAATATACCAGAAGTAG	ACGA**CCGCGG**CAGTGACAAAAGACGAGC
15	5′ *p2xD*	TGCA**GGGCCC**TTTTGGACGCTTTC	AGAT**AAGCTT**AAACTAGCCCTTATACTACCAAC
16	3′ *p2xD*	TAGA**GCGGCCGC**TCATGGTTTCTCTGAAAGTAG	ACAA**CCGCGG**AAGTTACAAATGACCCTTATG

dual ramp voltage protocol described above. Theoretical reversal potentials at different chloride concentrations were estimated using the Goldman-Hodgkin-Katz equation assuming intracellular concentrations of Cl^- (33.4 mM), K^+ (92.5 mM), and Na^+ (6.2 mM) were similar to those previously determined for *Xenopus* oocytes by Barish (12). Relative permeability (P_{K^+}/P_{Na^+}) values of 1.10 and 0.98, (as calculated above (Table 4)) were used for dP2XA and dP2XB, respectively.

Dictyostelium Culture and Transformation—Ax2 *Dictyostelium* and transformants were grown axenically in HL-5 media at 22 °C. Growth medium of strains expressing apoaequorin (pPROF120 plasmid (13)), dP2X-eGFP, dP2X-RFP, or vatM-GFP (pDXA/VatM-GFP (14)) was supplemented with 30 μg/ml G418 and for *p2x* null mutants with 10 μg/ml blasticidin S. Cell transformations were essentially as described previously (10).

Gene Disruption—The *p2xB*, *p2xC*, and *p2xD* single, and *p2xA/B/C/D/E* quintuple null strains were produced in Ax2 by homologous recombination using disruption vectors based on pLPBLP (15). Flanking homology regions were generated by PCR using primer pairs 11–16 (Table 1) and cloned on either side of the blasticidin S resistance cassette (bsr) via the exogenous restriction endonuclease sites introduced by the primers during amplification (5′ ApaI-HindIII and 3′ NotI-SacII). Disruption cassettes were liberated as ApaI/SacII fragments, and 15 μg was used to transform Ax2 *Dictyostelium*. Independent null strains were isolated from 96-well tissue culture plates in axenic medium plus 10 μg/ml blasticidin S as the selective agent. Gene disruptants were identified by PCR, using oligonucleotides located outside the disruption cassette and within bsr, with Southern blot analysis performed to verify a single site of integration (supplemental Fig. S1). To generate the quintuple *p2xA/B/C/D/E* knock-out strain bsr was recycled by transient expression of Cre recombinase (pDEX-NLS-cre (15)). Recombinants were isolated following 3–6 days selection in 30 μg/ml G418. Accurate recombination was verified by PCR, using oligonucleotides located either side of bsr.

Southern Blot Analysis—HindIII- or EcoRV-digested genomic DNA was probed with α-[^{32}P]dCTP-labeled SacI-HindIII-restricted bsr. Hybridization was as described in a previous study (10).

Aequorin Assays—In vivo reconstitution of aequorin was achieved as described previously (10). Luminescence signals were recorded between 1 and 2 h after aequorin reconstitution using a custom built luminometer (Cairn Research UK), with 1.5 ml of stirred cell suspension. Agonists or lysis solution (75 μl) were delivered using the auto-injector of the luminometer so as to standardize the speed and force of injection between experiments. For each experiment the total cell aequorin content was determined in at least 5 aliquots of cells by injecting lysis solution (10 mM MOPS, 10 mM calcium acetate, 0.5% Triton X-100, pH 7.0) to compare response magnitudes between experiments and strains as percent total aequorin consumption. Responses were analyzed using WinWCP software (Dr. J. Dempster, University of Strathclyde, Scotland) to determine peak area prior to determination of EC_{50} values using GraphPad Prism software.

Generation of dP2XB–E eGFP/RFP-expressing Strains—Strains expressing eGFP- or RFP-tagged dP2XB, dP2XC, dP2XD, and dP2XE (pDXA/dP2XB-eGFP and pDXA/dP2XB–E-RFP) were produced in Ax2 using expression vectors based on pDXA (16). dP2XB–E coding regions integrating an exogenous 5′ AAAAA sequence (17, 18) were generated by PCR using primer pairs 6–9 (Table 1). eGFP was digested from the plasmid pEGFPN1 (Clontech) as a BamHI-XbaI fragment, and mRFPmars was amplified by PCR from plasmid 339-3 (19) with primer pair 10 (Table 1). eGFP or RFP sequences were ligated at the C terminus of dP2X sequences, and the complete construct was cloned into pDXA utilizing restriction sites introduced by the PCR primers (BamHI and HindIII-XbaI, respectively).

A STREP II tag with a two-amino acid spacer (LE**WSHPQFEK)** was introduced into the predicted dP2XA inter-transmembrane domain between positions Thr^{71} and Phe^{72}. dP2XA Met^1–Thr^{71} and Phe^{72}–Leu^{378} coding regions were amplified by PCR using the following primer pairs: Met^1–Thr^{71} forward, 5′-TGGT**AAGCTT**AAAAAATGGGTTTTAGTTTTGATTGG-3′ and Met^1–Thr^{71} reverse, 5′-GGGG**CTCGAG**AGTATTTGGACCTTTTAAACTTG-3′; Phe^{72}–Leu^{378} forward, 5′-CCCC**CTCGAG**TGGAGCCACCCGCAGTTCGAAAAATTTGCATCAAATTTAACATATTG-3′ and Phe^{72}–Leu^{378} reverse, 5′-CCCC**GGATCC**AATAAACCTT-

CAATTCTTGTATATAAAAC-3′. The Phe[72]–Leu[378] forward primer incorporated the STREP II tag. The two PCR products were ligated utilizing exogenous XhoI restriction sites introduced by the PCR primers and cloned into pDXA/dP2XD-eGFP (HindIII-BamHI).

Confocal Microscopy—Confocal images were taken with a Leica TCS SP2 laser scanning microscope. Cells were preincubated in LoFlo medium (9) to reduce auto-fluorescence, and imaged in LoFlo medium diluted 1:2 in KK_2 buffer (16 mM KH_2PO_4, 4 mM K_2HPO_4).

Protease Protection Assay—The orientation of dP2X receptors in intracellular organelle membranes was determined using a protease protection assay on tagged dP2X receptors. Cells from axenic cultures were washed twice in proteinase K digestion buffer (20 mM Tris, 2 mM $CaCl_2$, pH 7.5) before resuspending at 1×10^8 cells/ml. Cells were then forced through a double layer of 5-μm filters twice, which was sufficient to disrupt the cell membrane of the majority of cells while leaving the membranes of intracellular organelles intact. Undisrupted cells were pelleted by centrifugation ($425 \times g$, 5 min, and 4 °C), and intracellular organelles were enriched from the supernatant by further centrifugation at $18{,}000 \times g$ for 10 min at 4 °C. Pelleted organelles were then resuspended in proteinase K digestion buffer (2 μg of protein/μl) and digested with proteinase K (100 μg/ml) for 30 min at 22 °C. Control total protein digestion with proteinase K was achieved following lysis of organelle membranes with 1% Triton X-100. Proteinase K-digested protein (typically 25 μg) was mixed 50:50 with gel sample buffer (50 mM Tris-Cl, pH 6.8, 200 mM dithiothreitol, 2% SDS, 10% glycerol), heated for 2 min at 70 °C, separated on a 10% SDS-PAGE gel before transfer to nitrocellulose. The membrane was incubated with anti-GFP antibody (1:10,000 dilution, Sigma) in PBST (1× PBS, 0.1% Tween 20)/5% milk powder for 2 h or with anti-STREP antibody (1:2000 dilution, Qiagen) in TBS (2 mM Tris-Cl, pH 7.5, 15 mM NaCl)/5% milk powder for 2 h and washed with PBST (3 × 10 min) or TBST (1× TBS, 0.05% Tween 20, 2 × 10 min) and TBS (1 × 10 min), respectively. Membranes were subsequently incubated with anti-mouse horseradish peroxidase secondary antibody (1:2,000 dilution, Dako, Denmark) in PBST or TBS/5% milk powder for 45 min and washed with PBST (2 × 10 min) and PBS (2 × 10 min) or TBST (4 × 10 min), respectively. Visualization of the protein bands was achieved with an ECL (Plus) kit (Amersham Biosciences) according to the manufacturer's instructions.

Osmoregulation Assay—Wild-type and *p2x* knock-out cells grown in HL5 media were transferred to 3-cm culture dishes and allowed to settle for 20 min. Reference differential interference contrast images were taken using a Nikon Eclipse Ti-S microscope (20× objective) and Openlab software before replacement of HL5 media with distilled water after two brief washes in distilled water. Differential interference contrast images were then collected at 5-min intervals, and cell area was subsequently measured for the same 20–40 cells from each image using ImageJ analysis software.

Data Analysis—Data are presented as means ± S.E. Differences between means were assessed by analysis of variance followed by Dunnett's post test (GraphPad Prism software).

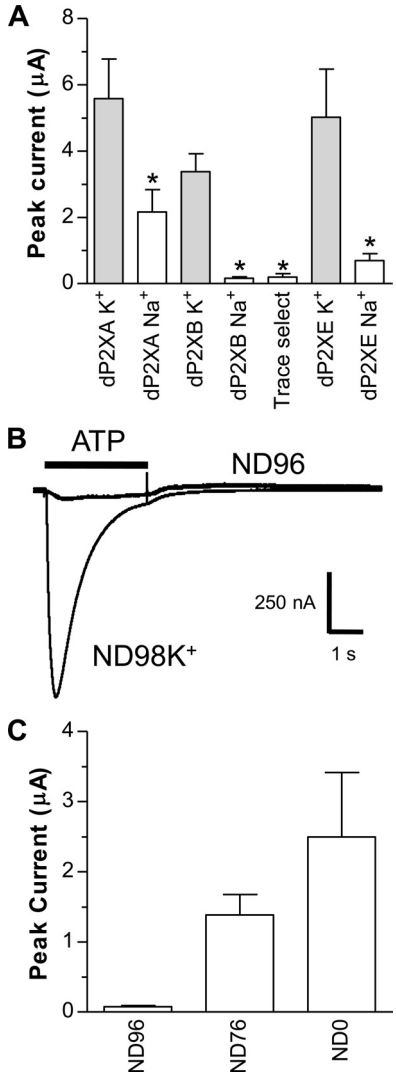

FIGURE 1. **dP2X receptors are inhibited by Na^+.** Two-electrode voltage clamp recordings at a holding membrane potential of −70 mV were made from *Xenopus* oocytes expressing dP2X receptors. *A*, comparison of peak current amplitudes recorded in response to 3 mM ATP in extracellular recording solutions consisting either of ND96 (Na^+ based) or ND98K^+ (K^+ based) with both solutions at pH 6.2. Note inhibition of currents by Na^+ particularly for dP2XB and dP2XE channels. "*Trace select*" denotes ND96 extracellular recording solution made with ultrapure NaCl (Fluka 38979) for dP2XB. *, significant difference, $p < 0.05$, compared with respective ND98K^+ current ($n = 7$). *B*, direct comparison of current amplitudes in ND96 and ND98K^+ extracellular recording solutions (both pH 6.2) in the same dP2XB-expressing oocyte. Application of ATP (3 mM indicated by the *bar*) in ND96 was followed 5 min later by ATP application in ND98K^+. *C*, mean current amplitudes in dP2XB-expressing oocytes after substitution of Na^+ in ND96 with NH_4^+. *ND76* denotes ND96 with 20 mM NH_4Cl substituting for 20 mM NaCl. *ND0* denotes solution with zero Na^+ and 96 mM NH_4Cl ($n = 7$).

RESULTS

Cloning of Dictyostelium P2X Receptor cDNAs—Reverse transcription-PCR on cDNA prepared from vegetative Ax2 cells using primers for the five *Dictyostelium* P2X receptor genes (Table 1) yielded cDNA clones that were a 100% match to the Dictybase-predicted coding sequence for *p2xA*, *p2xB*, and *p2xC*. Clones for *p2xD* differed from the Dictybase sequence at three codons, Asp[95] (GAT), Val[107] (GTT), and Asn[403] (AAT), in the Dictybase sequence were GGT (Gly), GAT (Asp), and AGT (Ser), respectively, in two independent PCR products

cloned for *p2xD*. Two independent clones sequenced for *p2xE* had a silent mutation from the predicted Dictybase sequence at codon P339 (CCC in Dictybase sequence *versus* CCA in cDNA clones).

ATP-evoked Currents in Xenopus Oocytes Expressing dP2X Receptors—Due to their very low sequence homology with vertebrate P2X receptors, it was not known whether, similar to dP2XA (5), the other four members of the *Dictyostelium* P2X-like family also exhibit P2X channel function. Here we show that dP2XB and dP2XE also represent ATP-gated ion channels and further characterize the permeation properties of dP2XA. No nucleotide-evoked currents, however, could be recorded from dP2XC- or dP2XD-expressing oocytes tested under a range of extracellular recording solutions and pH. The typical extracellular recording solution for the study of P2X ion channel function in *Xenopus* oocytes is ND96 (pH 7.5) with 1.8 mM $BaCl_2$ replacing the 1.8 mM $CaCl_2$ to prevent activation of endogenous calcium-activated chloride channels (20). In initial experiments using this solution with dP2XB- or dP2XE-expressing oocytes we obtained no or very small (<50 nA) currents upon ATP application (tested up to 3 mM). Substitution of $BaCl_2$ with $CaCl_2$ or omission of $MgCl_2$ in ND96 had no effect on these very small current amplitudes. ND96 with a more acid pH (pH 6.2) produced slightly larger currents (Fig. 1*A*), but these were still small (160 ± 45 nA for dP2XB and 696 ± 211 nA for dP2XE) in comparison to other non-vertebrate P2X channels expressed in *Xenopus* oocytes (4, 7). Surprisingly, when Na^+ was replaced with either NH_4^+ or K^+ in the extracellular recording solution current amplitudes became much larger (~3–6 μA) (Fig. 1) suggesting that dP2XB and dP2XE channels either have low Na^+ permeability or that Na^+ in some way inhibited the efficacy of ATP to activate the channel. Similar to dP2XB and dP2XE, currents through the dP2XA channel were also significantly larger ($p < 0.05$) when Na^+ was replaced with K^+ (Fig. 1), however Na^+ inhibition in dP2XA was less pronounced than in dP2XB or dP2XE. All chemicals were of analytical grade (SigmaUltra) nevertheless, to confirm that Na^+ inhibition was not due to trace contamination of metal ions, "trace select" NaCl (Fluka 38979) was also used for dP2XB-expressing oocytes, and the Na^+ inhi-

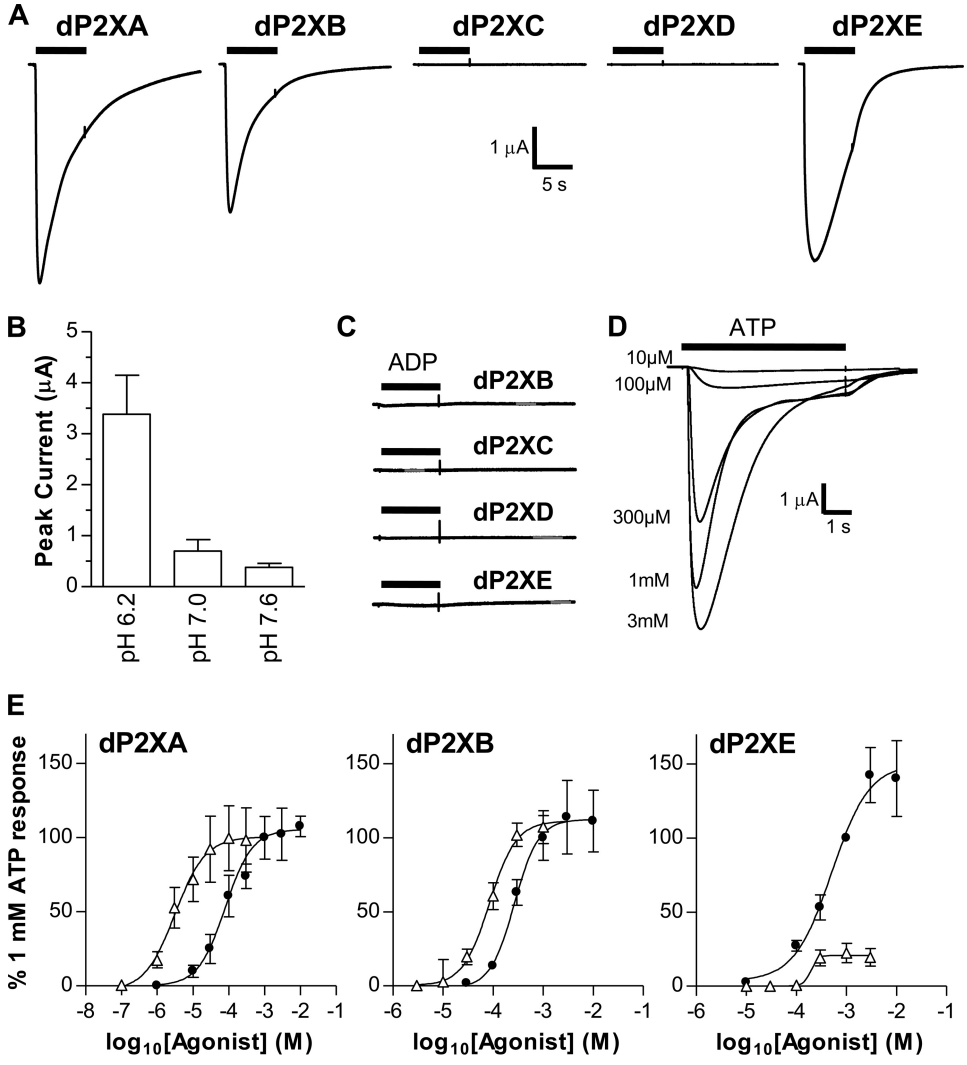

FIGURE 2. **ATP-evoked currents in dP2X receptors.** Two-electrode voltage clamp recordings from *Xenopus* oocytes expressing dP2X receptors. Agonist applications are indicated by *bars*. *A*, example membrane currents in dP2X-expressing oocytes recorded in response to 3 mM ATP. Extracellular recording solution was $ND98K^+$. ATP resulted in inward currents that decayed during the continued presence of agonist in dP2XA, dP2XB, and dP2XE receptors. No currents were detected for dP2XC- and dP2XD-expressing oocytes. *B*, effect of pH on dP2XB currents recorded in $ND98K^+$ ($n = 5$). *C*, dP2XB, -C, -D, and -E receptors are unresponsive to ADP (tested at 3 mM). *D*, example concentration-dependent currents for ATP in a dP2XE-expressing oocyte (application were 5 min apart). *E*, concentration response curves for ATP (*black circles*) and β,γ-imido-ATP (*white triangles*) in dP2XA-, dP2XB-, and dP2XE-expressing oocytes. Mean currents (±S.E.) were normalized to the response given by 1 mM ATP ($n = 7$ oocytes for dP2XE and 10–15 oocytes per data point for dP2XA and dP2XB).

TABLE 2
Properties of ATP evoked currents in *Dictyostelium* P2X channels

Channel	Peak current	EC_{50}	pEC_{50}	Hill slope	0–100% Rise time	50% Decay time
	nA	*μm*			*ms*	*ms*
dP2XA	−2405 ± 777	97	4.01 ± 0.07	0.94 ± 0.11	313 ± 60	2115 ± 423
dP2XB	−1371 ± 372	266	3.56 ± 0.04	1.81 ± 0.28	1092 ± 120	2130 ± 170
dP2XE	−5219 ± 1076	511	3.29 ± 0.04	1.15 ± 0.32	1566 ± 283	3487 ± 442

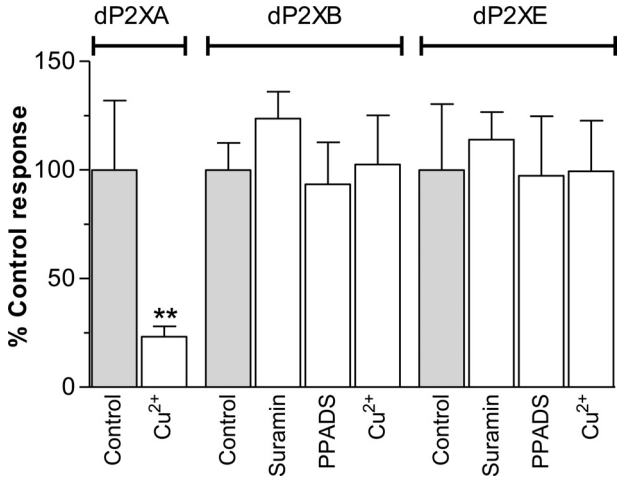

FIGURE 3. **dP2XB and dP2XE receptors are not inhibited by copper, suramin, or PPADS.** Peak current responses for each receptor were normalized to the mean of the control response to 3 mM ATP with no inhibitor present (n = 6–10 oocytes for each data point). $CuCl_2$ (100 nM), suramin (100 μM), or PPADS (100 μM) were present in both the bath solution (5-min incubation prior to agonist application) and the 3 mM ATP solution. Unlike dP2XA (5) (**, $p < 0.01$), dP2XB and dP2XE are not inhibited by nanomolar concentrations of copper, and neither receptor is sensitive to the common P2 receptor antagonists PPADS and suramin.

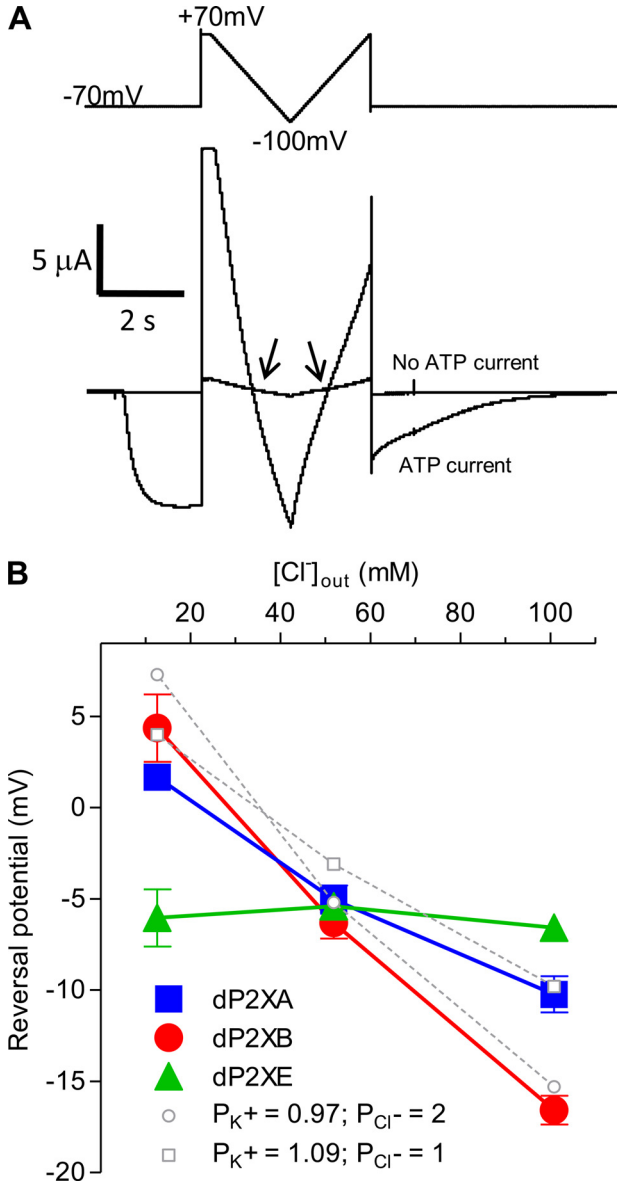

FIGURE 4. **dP2XA and dP2XB are permeable to chloride ions.** Reversal potentials were determined in external solutions with differing [Cl^-] by substitution of KCl with potassium gluconate so as to keep [K^+] constant while lowering [Cl^-]. *A*, examples of current traces for dP2XB in 98 mM KCl. The reversal potential was taken as the mean value of the two crossover points (*arrows*) between the current in the absence of ATP and the current in the presence of ATP (3 mM). The voltage ramp protocol is indicated *above* the *current trace*. *B*, plot of reversal potential against [Cl^-]. Note the reversal potential for dP2XE is not affected by changes in [Cl^-], whereas with dP2XA and dP2XB reversal potential becomes more positive with decreasing [Cl^-]. Values are plotted as mean ± S.E., $n > 6$ from at least two independent experiments for each data point. Theoretical reversal potentials (*dotted lines*) for the experimental chloride concentrations were estimated using the Goldman-Hodgkin-Katz equation (see "Experimental Procedures") using relative (P_{K^+}/P_{Na^+}) values of 1.10 and 0.98 (as calculated in Table 4) for dP2XA and dP2XB, respectively.

bition remained (Fig. 1*A*). In the absence of Na^+ ions, pH also affected current amplitudes with acidic pH (6.2) producing significantly larger current amplitudes than neutral or slightly alkaline pH (Fig. 2*B*). In subsequent experiments to further characterize the properties of dP2X channels we therefore routinely used extracellular recording solution with K^+ substituting Na^+ and a pH of 6.2 (ND98K^+, see "Experimental Procedures").

ATP evoked inward currents in dP2XA-, dP2XB-, and dP2XE-expressing oocytes that decayed during the continued presence of agonist (Fig. 2*A*) and showed EC_{50} values of 97, 266, and 511 μM, respectively (Fig. 2*E* and Table 2). The time course of ATP responses at the three channels was quite similar, and current decay (measured as time from peak current to 50% peak) was not significantly different. Currents through dP2XA channels however had a faster rise time ($p < 0.01$) than either dP2XB or dP2XE (Table 2). β,γ-Imido-ATP has previously been reported to be a more potent agonist than ATP at dP2XA (5). Similarly, under our experimental conditions β,γ-imido-ATP was ~30-fold more potent at dP2XA with an EC_{50} of 3.1 μM. We therefore tested this ATP analogue on the other four dP2X receptors. β,γ-Imido-ATP was a full agonist at dP2XB and was 3-fold more potent than ATP with an EC_{50} of 85 μM. In contrast to dP2XA and dP2XB, β,γ-imido-ATP was a weak partial agonist at dP2XE producing a maximal response only 22.3 ± 6.4% that of ATP (Fig. 2*D*). Similar to ATP, β,γ-imido-ATP produced no response at dP2XC and dP2XD. We also tested UTP, UDP, UMP, uridine, GTP, GDP, GMP, guanosine, CTP, CDP, CMP, cytidine, ADP, AMP, adenosine, cAMP, and cGMP (all at 300 μM) at all five dP2X receptors. None of these potential agonists produced currents in any of the dP2X receptors demonstrating that dP2XA, dP2XB, and dP2XE are highly selective for ATP.

Effects of PPADS, Suramin, and Copper at dP2XB and dP2XE—The general P2 receptor antagonists suramin and PPADS have previously been shown to be ineffective at dP2XA (5). Similarly, currents through dP2XB and dP2XE were also not affected by either compound tested at concentrations up to 100 μM in *Xenopus* oocytes (Fig. 3). dP2XB and dP2XE did, however, differ from dP2XA in their sensitivity to copper. dP2XA currents when expressed in HEK293 cells are blocked by nanomolar concentrations of copper (IC_{50} 40 nM) (5). A similar inhibition

TABLE 3
Reversal potential of ATP evoked currents in different extracellular recording solutions

Channel	98 mM K^+	98 mM Na^+	98 mM NH_4^+	98 mM choline	49 mM gluconate	88.2 mM gluconate
				mV		
dP2XA	−10.2 ± 1.0	−12.6 ± 0.9	4.0 ± 1.5	−29.4 ± 2.3	−5.0 ± 0.8	1.7 ± 0.6
dP2XB	−16.6 ± 0.8	−15.8 ± 0.7	0.6 ± 1.3	−30.0 ± 5.0	−6.3 ± 0.9	4.4 ± 1.8
dP2XE	−6.6 ± 0.6	−17.6 ± 1.0	−2.90 ± 1.3	−32.1 ± 1.8	−5.4 ± 0.5	−6.0 ± 1.6

TABLE 4
Permeability ratios of different ions through *Dictyostelium* P2X channels

Channel	P_{K^+}/P_{Na^+}	P_{NH4^+}/P_{Na^+}	$P_{choline}/P_{Na^+}$
dP2XA	1.10 ± 0.04	1.97 ± 0.12	0.52 ± 0.04
dP2XB	0.98 ± 0.03	1.93 ± 0.09	0.63 ± 0.07
dP2XE	1.56 ± 0.04	1.81 ± 0.09	0.57 ± 0.04

for dP2XA by copper was observed in *Xenopus* oocytes, however copper had no effect on currents through dP2XB and dP2XE (Fig. 3). The macrocyclic lactone ivermectin, which has been shown to potentiate P2X receptor currents in human and rat $P2X_4$ receptors (20, 21), and invertebrate P2X receptors from *Schistosoma mansoni* (4) and *Hypsidius dujardini* (7) had no effect on the *Dictyostelium* dP2XA, -B, or -E receptors (data not shown).

Relative Permeability of Cations through dP2X Receptors—Currents through dP2XB and dP2XE are small when Na^+ was the major cation in the extracellular recording solution (Fig. 1*A*) and to determine whether this was due to a low Na^+ permeability we determined reversal potentials of dP2X receptors in different extracellular solutions by applying a dual ramp protocol from +70 to −100 mV in the presence and absence of 3 mM ATP (Fig. 4*A*). Changes in reversal potential were used to calculate the relative permeability ratio of the test cation to Na^+ (see "Experimental Procedures"). As control we used the human $P2X_2$ receptor and obtained a permeability ratio for P_{K^+}/P_{Na^+} of 1.05 ± 0.04 (n = 8), which is consistent with previously published data (22). P_{K^+}/P_{Na^+} values for dP2X receptors were 1.10 ± 0.04, 0.98 ± 0.03, and 1.56 ± 0.04 for dP2XA, dP2XB, and dP2XE, respectively, showing that low Na^+ permeability was not the underlying cause of current inhibition in dP2XB and dP2XE currents recorded in ND96 solution. dP2X receptors were more permeable to NH_4^+ than either Na^+ or K^+ ions and less permeable to choline (Table 4).

dP2XA and dP2XB Receptors Are Permeable to Chloride—The relatively negative reversal potentials for dP2XA and dP2XB in 98 mM K^+ compared with dP2XE (Table 3) suggested differences in ionic permeability. We therefore investigated the possibility of chloride permeability in dP2X channels by substitution of KCl in the extracellular recording solution with potassium gluconate thereby reducing $[Cl^-]_{out}$ while $[K^+]_{out}$ remained constant. If a channel is impermeable to Cl^- then reduction of $[Cl^-]_{out}$, while the concentration of other permeable ions remains constant, would not be expected to alter the reversal potential. This was the case for dP2XE where a plot of reversal potential against $[Cl^-]_{out}$ essentially produced a horizontal line (Fig. 4*B* and Table 3) showing that dP2XE is not permeable to Cl^-. With dP2XA and dP2XB, however, reversal potentials shifted to more positive values with decreasing concentrations of $[Cl^-]_{out}$ demonstrating Cl^- permeability in these channels. As an estimate of the relative Cl^- permeability for dP2XA and dP2XB we used the Goldman-Hodgkin-Katz equation to calculate theoretical shifts in reversal potential given relative permeability values for dP2XA and dP2XB of 1.10 and 0.98 (Table 4), respectively. For dP2XA a relative chloride permeability of 1 gave a close correlation to the experimental data while for dP2XB a relative Cl^- permeability of 2 was required to match the experimental data (*dotted lines*, Fig. 4*B*).

The Extracellular Purinergic Response Remains after Ablation of all Five p2x Genes—By using single gene ablation, we previously ruled out dP2XA and dP2XE as the cell surface receptors exclusively mediating the *Dictyostelium* calcium response to extracellular purine nucleotides (10). We therefore generated knock-out strains for the *p2xB*, *p2xC*, and *p2xD* genes to complete the set of individual gene knock-outs for the five *Dictyostelium* P2X receptors. We also generated a quintuple knock-out strain (*p2xA/p2xB/p2xC/p2xD/p2xE-*) devoid of any dP2X receptors by sequentially disrupting all five *p2x* genes. No obvious morphological phenotype was apparent in any of the single or quintuple *p2x* null strains. Cells grew in both HL5 media and on bacterial plates and were also able to develop normally upon starvation to form fruiting bodies. The quintuple *p2x* null strain, however, did grow slightly slower than wild type in shaking axenic cultures with a doubling time ~40% greater than wild type.

Responses to extracellular ATP persisted in *p2xB*, *p2xC*, and *p2xD* single null strains with no alteration in the kinetics of the response (Fig. 5*A*) or potency (pEC_{50} = 5.49 ± 0.03, 5.56 ± 0.03, 5.45 ± 0.03, and 5.49 ± 0.02 for *p2xB*, *p2xC*, *p2xD*, and WT strains, respectively) (Fig. 5*B*). The absolute magnitude of responses, however, expressed as a percentage of total aequorin consumption, were 26- 50% lower in single *p2x* null strains compared with wild type (Fig. 5*D*).

To rule out the possibility of functional compensation from remaining dP2X receptors in the single null strains we also assayed the quintuple knock-out strain, which lacked all five dP2X receptors. Again the endogenous response to extracellular ATP persisted in this quintuple (*p2xA/p2xB/p2xC/p2xD/p2xE*) knock-out with no change in potency (pEC_{50} = 5.62 ± 0.03) (Fig. 5*B*) and a similar time course of the response (Fig. 5*A*). Similarly, the equipotency of ADP to ATP was maintained in all single and the quintuple knock-out strains. However, the reduction in response magnitude observed in the single *p2x* null strains was greater in the quintuple knock-out with a 66% reduction in magnitude compared with wild type (Fig. 5*D*). This reduction in response magnitude could potentially be explained by the removal of ATP/ADP-sensitive dP2X receptors at the cell surface, or alternatively due to disruption of subsequent downstream intracellular calcium signaling mediated by dP2X receptors but initiated by the activation of a non-P2X cell

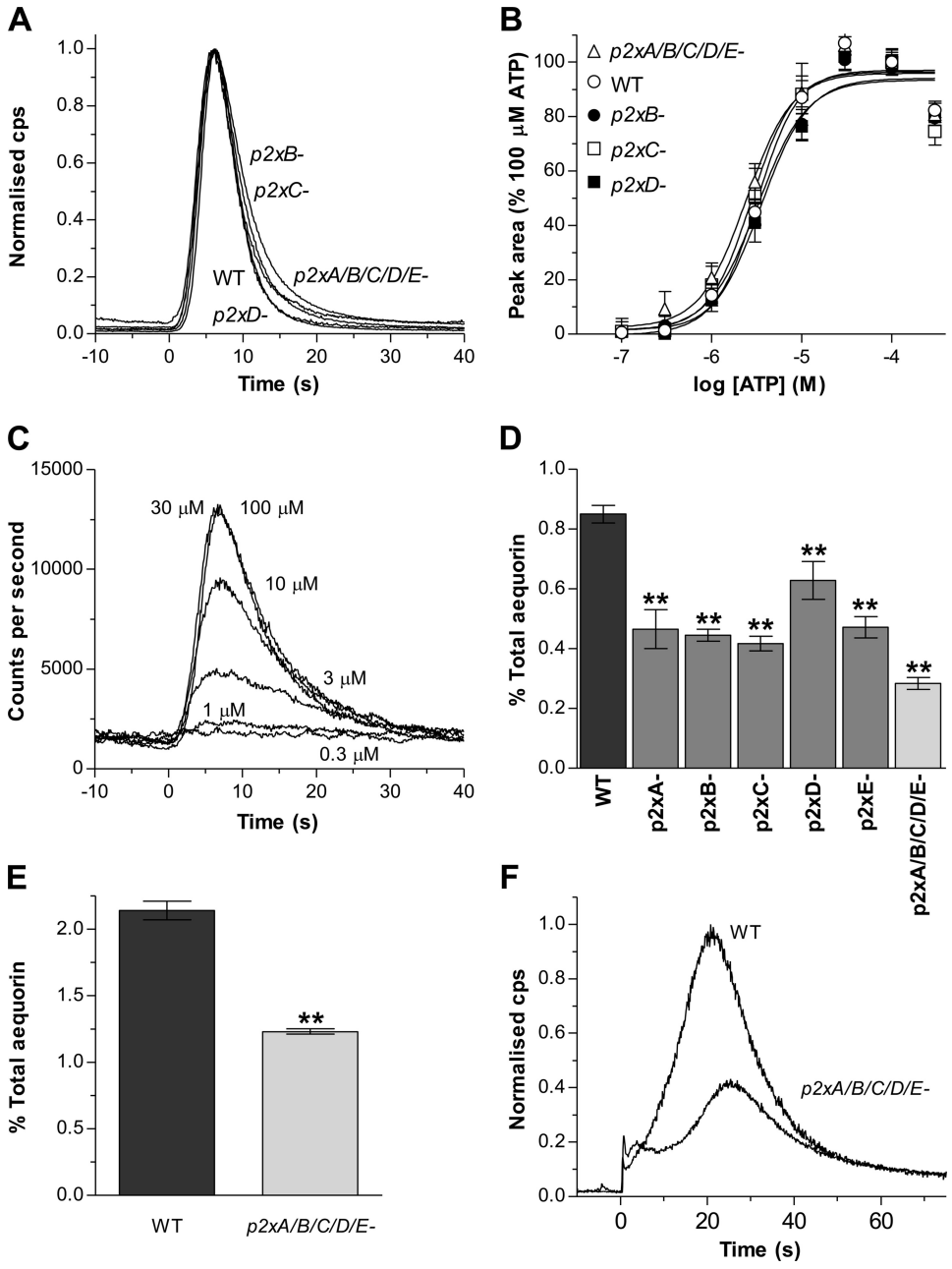

FIGURE 5. **The response to extracellular purine nucleotides persist in *p2x* null strains.** *A*, representative aequorin responses to ATP (30 μM) in *p2xB*, *p2xC*, and *p2xD* single and *p2xA/B/C/D/E* quintuple null strains compared with wild type (*WT*). Cells were incubated with the cofactor benzyl-coelenterazine in HL-5 media (1×10^7 cells/ml) to reconstitute functional aequorin and then transferred to MES development buffer (10 mM MES, 10 mM KCl, 0.25 mM $CaCl_2$ pH 6.8) (5×10^6 cells/ml), and responses to ATP were monitored using a luminometer. The kinetics of the response to ATP is unaffected by *p2x* gene deletion. Traces are normalized to the maximal response for each individual strain to provide a direct comparison of time course. Time 0 corresponds to the application of agonist. *B*, ATP concentration response curves for WT and *p2x* null strains. Data are normalized to 100 μM ATP for each strain (mean ± S.E., $n \geq 5$ for each data point from at least two independent experiments). *C*, representative concentration-dependent ATP responses in *p2xA/B/C/D/E* quintuple null cells. *D*, response magnitudes to ATP (30 μM) expressed as percent total aequorin consumption for wild-type (*WT*) and *p2x* null strains. Data are presented as means ± S.E. from 18 independent experiments for wild-type and six independent experiments with two independent clones for *p2x* null strains ($n \geq 30$). *E*, the magnitude of the response to calmidazolium (2.5 μM) is reduced in *p2xA/B/C/D/E* quintuple null cells compared with wild type (*WT*). Data are presented as mean percent total aequorin consumption from four independent experiments with two independent clones assayed for *p2xA/B/C/D/E* null cells ($n \geq 20$). *F*, representative aequorin responses to calmidazolium (2.5 μM) in wild-type and *p2xA/B/C/D/E* null cells. **, significant difference ($p < 0.01$) compared with wild type.

surface purinergic receptor. To address this issue further we looked at responses to calmidazolium (R24571) in aequorin-expressing cells, because this calmodulin inhibitor is known to induce calcium release from intracellular stores in *Dictyostelium* (23). Similar to ATP/ADP responses, the response to calmidazolium was also reduced in quintuple *p2x* null cells compared with wild type (Fig. 5, *E* and *F*) suggesting that the absence of the dP2X proteins results in disruption of intracellular calcium signaling.

All Five dP2X Proteins Show an Intracellular Localization to the Contractile Vacuole—Given that the extracellular purinergic response persists in the complete absence of dP2X receptors, it is likely that, similar to dP2XA (5), the other four members of the *Dictyostelium* P2X family also represent intracellular receptors. To determine subcellular localization, strains overexpressing dP2XB–D receptors tagged with the fluorescent protein RFP were generated. Tagged dP2XB–D receptors all showed a preferential localization to the membranes of large intracellular vacuolar structures with no detectable levels of receptor expression at the plasma membrane (Fig. 6*A*). RFP-tagged dP2XB–E receptors all colocalized with eGFP-tagged vatM (Fig. 6, *B* and *C*), a subunit of the vH+ATPase enriched on the contractile vacuole membrane (14), demonstrating that similar to dP2XA (5), dP2XB, -C, -D, and -E receptors are also present on this osmoregulatory organelle.

Membrane Orientation of dP2X Receptors in Contractile Vacuoles—The orientation of dP2X proteins in the intracellular contractile vacuole membrane is currently unknown. The agonist binding domain could potentially face the cytoplasm or the vacuole lumen. To determine membrane orientation a STREP tag II was introduced into the predicted inter-transmembrane domain of dP2XA-eGFP so as to provide a dual-tagged construct with different immuno-detectable epitopes on either side of the membrane (Fig. 7*A*). The cellular distribution of this dual-tagged construct was comparable to that of dP2XA-eGFP, and importantly expression on vacuolar membranes was not disrupted (Fig. 7*C*). Intact

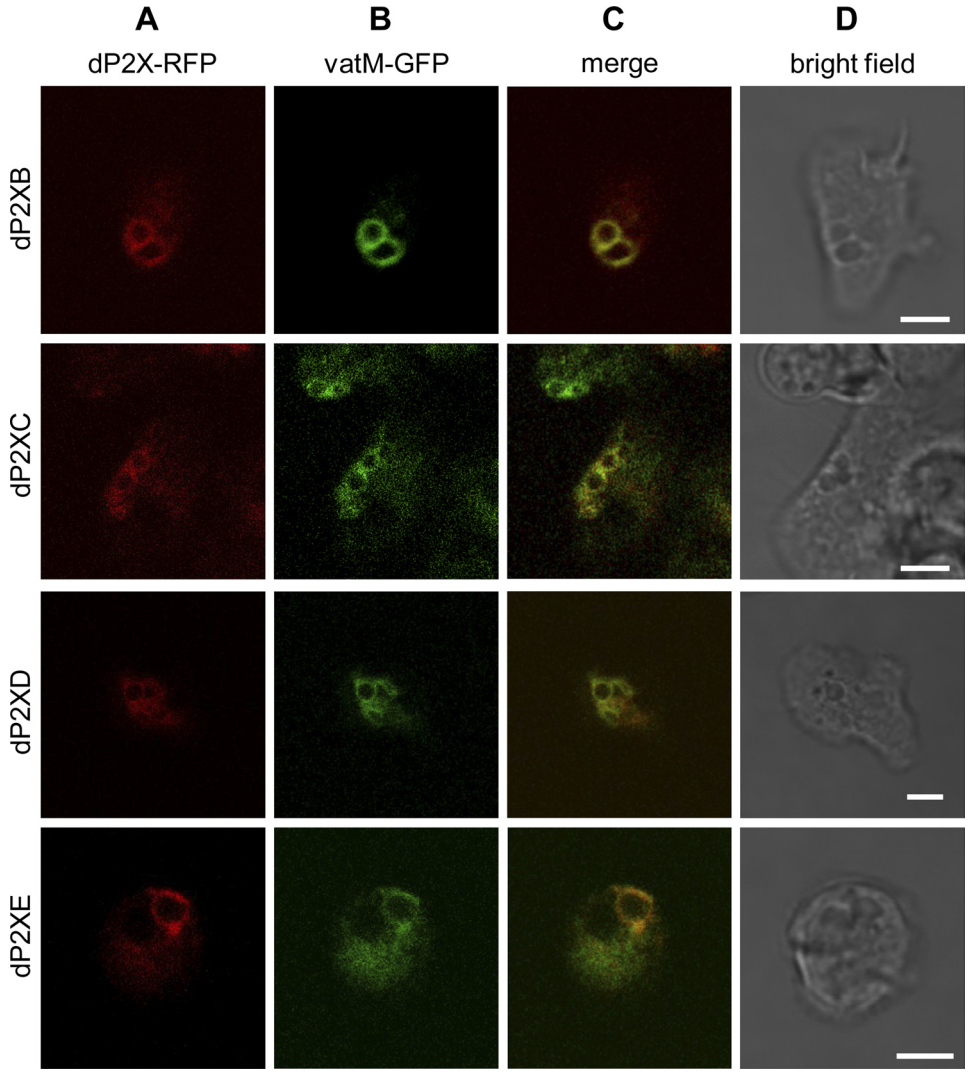

FIGURE 6. **Intracellular localization of dP2XB–E receptors.** Ax2 *Dictyostelium* co-transformed with RFP-tagged dP2XB–E receptors and eGFP-tagged vatM (14) were visualized by confocal microscopy. RFP-tagged dP2XB–E receptors localized to membranes of an intracellular organelle (*Column A*) with no detectable expression on the plasma membrane. eGFP-tagged vatM, which corresponds to the 100-kDa subunit of the contractile vacuole vH+ATPase (14) localized to the same intracellular membranes as RFP-tagged dP2X receptors (*Columns B* and *C*), showing that dP2X receptors are enriched on the membranes of the contractile vacuole. *Scale bars*, 5 μm.

intracellular organelles were exposed to proteinase K to digest exposed protein domains while keeping those domains present within the organelle protected from protease activity. Western blot analyses of the products of protease treatment using anti-STREP or anti-GFP antibodies demonstrated that proteinase K was able to fully digest the C-terminal region of the receptor containing the eGFP tag while the inter-transmembrane loop encompassing the STREP tag remained protected (Fig. 7*D*). Prior treatment of vacuoles with Triton X-100 resulted in proteinase K digestion of both epitope tags, because disruption of the vacuole membrane will allow proteinase K accessibility to both the cytoplasmic and lumen sides of the vacuole. The orientation indicated by these results puts the predicted agonist binding site within the lumen of the vacuole and the N and C termini within the cytoplasm. In addition to a STREP-tagged digestion product corresponding in size to the full inter-transmembrane region (~30 kDa), a smaller product of ~20 kDa containing the STREP tag was also observed. This smaller band often represented the major of the two digestion products and occasionally, when a higher proteinase K:protein ratio was used (Fig. 7*D*, *gel 3*), was the only digestion product detected. The presence of this smaller ~20-kDa band suggests that part of the inter-transmembrane region is exposed to the enzyme in the extra-organelle environment, possibly via a re-entrant loop. Similar to dP2XA, protease protection assays on dP2XB-eGFP, dP2XC-eGFP, dP2XD-eGFP, and dP2XE-eGFP (Fig. 7*E*), demonstrated that the C-terminal domains of these constructs were also exposed to the cytoplasmic side of the vacuole membrane revealing an equivalent membrane orientation for all five dP2X proteins. In addition to GFP-tagged dP2X proteins, the anti-GFP antibody in some cases also recognized a smaller protein of ~30 kDa in undigested samples. The intensity of this band varied between samples, and its identity was not clear. The presence of this band, however, did not interfere with the interpretation of the proteinase K protection results.

dP2X Null Strains Are Still Capable of Osmoregulation—p2xA null *Dictyostelium* have previously been described to be incapable of regulating their volume in hypotonic conditions with cells continuing to swell rather than showing an osmoregulatory decrease in volume leading to the conclusion that dP2XA is required for osmoregulation (5). The *p2xA* and other single null strains described in this study, however, did not show any noticeable differences in their sensitivity to hypotonic conditions. Each single p2x null strain behaved in a similar manner to wild type, swelling initially over the first 10 min after exposure to water and then recovering their volume by 60 min. Even complete absence of all five dP2X receptors in the *p2xA/B/C/D/E* null strain did not prevent cells from undergoing osmoregulation. Like wild type, *p2xA/B/C/D/E* null cells swelled by 15–20% within the first 10 min of exposure to water before undergoing a regulatory decrease in cell volume (Fig. 8). There was, however, a delay of ~15 min in the onset of this regulatory decrease in volume in the *p2xA/B/C/D/E* cells, but the subsequent rate of volume decrease was very similar to wild-type cells (Fig. 8*C*). Similar to previous studies (5),

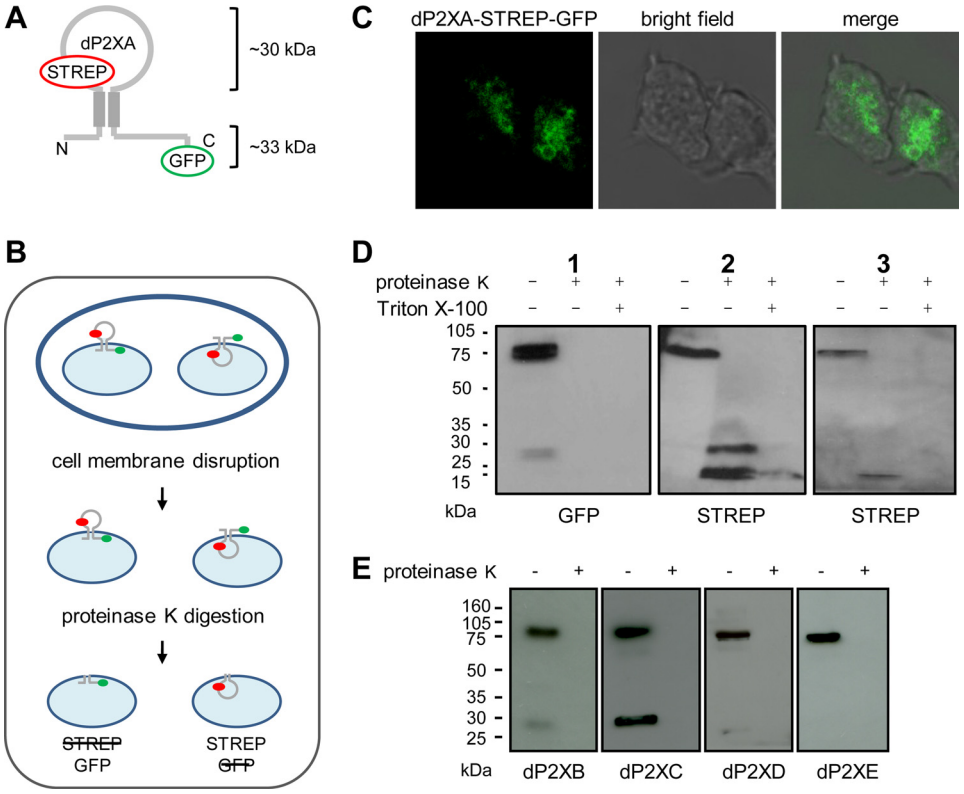

FIGURE 7. **Orientation of dP2X proteins in contractile vacuole membranes.** *A*, schematic of the dual-tagged dP2XA construct. Predicted sizes of fragments protected from proteinase K digestion are ~30 kDa for the inter-transmembrane loop region and ~33 kDa for the GFP-tagged C-terminal domain. *B*, overview of the protease protection assay. Cells were disrupted by passage through a 5-μm pore membrane so as to keep intracellular organelles intact prior to exposure to proteinase K (100 μg/ml). The inability of this enzyme to cross the membrane of intact organelles allows a distinction to be made between protein elements that reside in the cytosol (exposed proteinase K) and those that reside within the vacuole lumen (protected from proteinase K). The *left side* of the *diagram* depicts the scenario if the orientation was such that the inter-transmembrane domain is exposed to the cytosol (the STREP tag would be digested while the GFP tag would remain intact). The *right side* depicts the converse where the inter-transmembrane domain resides inside the vacuole lumen resulting in digestion of the GFP tag while STREP remains intact. *C*, representative confocal image of the dual-tagged dP2XA protein in vegetative cells confirming that contractile vacuole localization has not been disrupted by insertion of epitope tags. *Scale bar* is 5 μm. *D*, Western blot analysis of dual-tagged dP2XA incubated in the presence and absence of proteinase K. Both GFP and STREP epitopes are detectable in the full-length undigested receptor. However, after proteinase K digestion only the STREP epitope remains intact. A short pre-treatment with 1% Triton X-100, to disrupt vacuole membranes, permitted proteinase K access to the lumen and digestion of the STREP tag. An additional band containing the STREP epitope smaller than the expected ~30 kDa was also detected (*gels 2* and *3*). This band was often the most prominent of the two digestion products observed and in samples where a higher proteinase K:protein ratio was used represented the only band detected (*gel 3*). *E*, loss of the GFP epitope following proteinase K digestion of intact vacuoles containing dP2XB–eGFP confirms an equivalent orientation for all five receptors. In some undigested samples the GFP antibody also detected a lower molecular weight protein of unknown origin (prominent in dP2XC example gel and also visible in dP2XB gel and *gel 1*).

the presence of 10 μM copper prevented both wild-type and mutant cells from undergoing an osmoregulatory decrease in cell volume, and cells remained swollen after 60-min exposure to water (Fig. 8*B*).

DISCUSSION

In this study we provide direct electrophysiological evidence that two further members of the *Dictyostelium* P2X-like family (dP2XB and -E) function as ATP-gated ion channels. Given the low sequence similarity with vertebrate P2X receptors (between 8.5 and 18.8% amino acid identity with human $P2X_{1-7}$ receptors), it is remarkable that, similar to dP2XA, these two *Dictyostelium* P2X channels are still exclusively selective for ATP over other nucleotides. Whether the agonist binding site in the *Dictyostelium* P2X receptors is analogous to their vertebrate counterparts is uncertain. The recently solved crystal structure for zebrafish $P2X_4$ is in the agonist-unbound state (24), and the definitive localization of the ATP binding site therefore remains unknown. ATP binding in vertebrate P2X receptors is known to occur between adjacent subunits (24, 25) and is thought to involve lysine residues that coordinate phosphate binding (26), an NFR motif that binds adenine/ribose and an FT motif also involved in agonist action (27). Similarities in ATP binding for dP2XA and vertebrate P2X receptors have been demonstrated by site-directed mutagenesis where Lys^{67} (equivalent to human $P2X_1$ Lys^{70}) and Lys^{289} (equivalent to human $P2X_1$ Lys^{309}) both disrupted ATP evoked currents when mutated to alanine (5). However dP2XB lacks the first of these lysine residues and dP2XE lacks both lysines. It is therefore surprising that dP2XB and dP2XE are still gated by ATP given that the equivalent lysine residues in vertebrates are thought to coordinate binding of ATP phosphate moieties, suggesting that other regions of the receptor must also be important in agonist recognition.

An unusual property of the dP2X receptors, particularly dP2XB, is the inhibition of current amplitude by Na^+ (Fig. 1, *A* and *B*). The small currents in the presence of high Na^+ were not a result of low Na^+ permeability, because P_{K^+}/P_{Na^+} was shown to be ~1 (Table 4). It is therefore likely that Na^+ exerts some form of allosteric modulation on dP2X channel function possibly by affecting the mean open time by a mechanism similar to that proposed for human $P2X_7$ (28). Permeability to chloride is also an unusual feature for P2X receptors, however, this is not unique, because chicken and human $P2X_5$ receptors have also been shown to pass chloride ($P_{Cl^-}/P_{Na^+} = 0.5$) (11, 29). Interestingly, the dP2X receptors differed in their permeability to chloride with dP2XA and dP2XB being permeable but dP2XE not (Fig. 4). The relative permeability of Cl^- to Na^+ was estimated to be ~2 for dP2XB and ~1 for dP2XA. Although these values can only be taken as a rough estimate, because the actual intracellular concentrations of ions in the batches of oocytes used was not determined, the data clearly demonstrate that dP2XB is more permeable to Cl^- than dP2XA. The relevance of

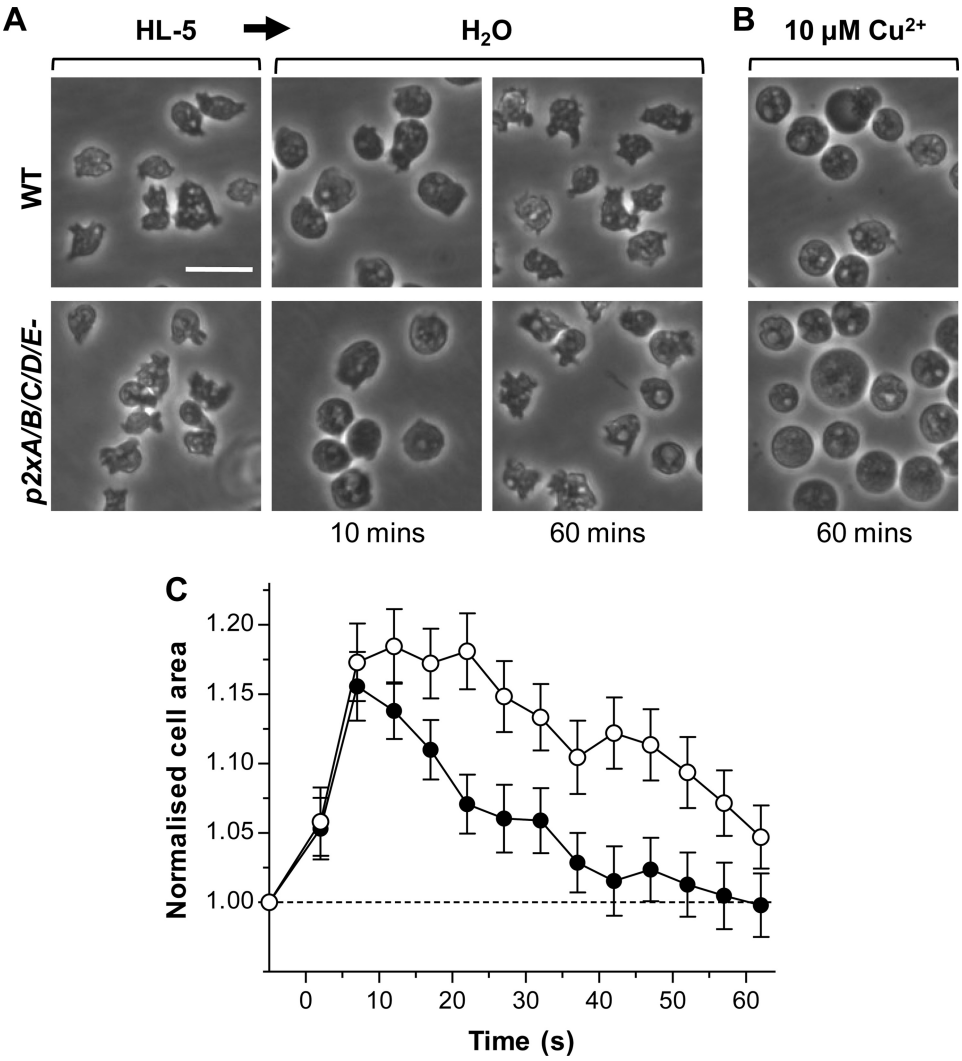

FIGURE 8. **dP2X receptors are not essential for osmoregulation.** *A*, differential interference contrast images of wild-type (*top panel*) and quintuple *p2x* null (*bottom panel*) cells in HL5 media and distilled water at 10 and 60 min. Both wild-type and mutant cells swell within the first 10 min and recover after 60 min. *B*, in the presence of 10 μM copper both wild-type and quintuple *p2x* null cells remain swollen after 60 min. *Scale bar*, 20 μm. *C*, time course of cell swelling and recovery in wild type (*black circles*) and quintuple *p2x* null (*white circles*) cells in distilled water. *p2x* null cells remain swollen slightly longer than wild type but are still able to recover. Data are presented as means of four independent experiments for wild type and six independent experiments with two independent clones (three experiments for each clone) for *p2x* null cells (n = 80–240 cells for each data point).

this Cl^- permeability is unclear, because the ionic composition of the contractile vacuole remains largely undetermined, although a vacuolar protein pump (14), the Ca^{2+} ATPase PAT1 (30), and the NH_4^+ transporter AmtB (31) have all been localized to the contractile vacuole membrane. In respect to the latter, the relatively high permeability of the dP2X proteins to NH_4^+ (Table 4) may have physiological significance.

The lack of functional currents in dP2XC or dP2XD could possibly be due to inappropriate post-translational processing of *Dictyostelium* proteins in *Xenopus* or gating of these channels by non-nucleotide ligands. Alternatively, dP2XC and dP2XD may require co-expression with other dP2X family members to form heteromeric channels (32, 33) or require the presence of one or more accessory proteins. Co-expression of dP2XC together with dP2XD in oocytes did not produce ATP/ADP-evoked currents, and co-expression of either channel with dP2XB resulted in a dominant negative phenotype with loss of ATP-gated currents (data not shown). Whether this dominant negative effect represents a physiological mechanism by which dP2XC/D can regulate the activity of the other dP2X proteins remains to be determined.

Colocalization of RFP tagged dP2XB–E with eGFP-tagged vatM (14) on the membranes of the contractile vacuole (Fig. 6, *B* and *C*), demonstrated that, similar to dP2XA (5), dP2XB, -C, -D, and -E receptors are also localized to this intracellular organelle. The low potency of ATP at dP2XA, -B, and -E receptors, ranging from EC_{50} ~100 to 500 μM (Table 2), is perhaps a reflection of this intracellular localization, because the concentration of ATP will typically be much higher within the cell than in the extracellular environment. Key to understanding the functional roles of dP2X receptors in contractile vacuole function is determining the membrane orientation, because this will provide information on both the potential origin of agonist activating the receptor and the regulatory/modulatory influences that the different domains of the receptor are exposed to. By using a protease protection assay on tagged receptors we demonstrated that the transmembrane loop region containing the agonist binding site lies within the lumen of the vacuole (Fig. 7). The source of ATP within the vacuole to activate these receptors, however, is currently unknown. One speculative possibility is that ATP containing vesicles within the cytoplasm could fuse with the vacuole membrane to release ATP into the lumen in a manner analogous to the exocytosis of ATP in vertebrate astrocytes (34). Such a mechanism would likely be regulated by calcium and could possibly involve the *Dictyostelium* SNARE protein Vamp7B, which has recently been shown to be present on the contractile vacuole membrane (35). Alternatively, analogous to plasma membrane pannexin 1 function in vertebrates (36), the vacuole membrane may contain channels capable of passing ATP from the cytoplasm to the vacuole lumen. It is also feasible, as has been recently demonstrated in phagosomes (37, 38), that active transport of ADP could occur across the vacuole membrane with subsequent conversion to ATP within the lumen.

The finding that all five members of the *Dictyostelium* P2X family have an intracellular localization was unexpected,

because these receptors were the most likely candidates for the cell surface receptor mediating the P2X-like calcium response evoked by extracellular ATP/ADP (10). Consistent with an intracellular rather than cell surface function for the entire dP2X receptor family, responses to extracellular ATP/ADP remained largely unaffected in the quintuple *p2x* knock-out strain with overlapping concentration response curves and time course of response (Fig. 5, *A* and *B*). A decrease in the magnitude of the extracellular purinergic response was observed in *p2x* null strains (Fig. 5*D*). However, it is unlikely that this decrease is a direct result of loss of dP2X channel activity at the cell surface, because the magnitude of the calcium response evoked by the calmodulin inhibitor calmidazolium was also decreased in the absence of dP2X receptors (Fig. 5*F*). A more likely explanation for the reduction in magnitude of both ATP/ADP and calmidazolium responses in *p2x* null strains is that dP2X receptors are involved in facilitating intracellular calcium signaling. The contractile vacuole is primarily an osmoregulatory organelle, however, recent studies have also suggested that it additionally acts as a Ca^{2+} store involved in intracellular Ca^{2+} signaling (39). It is therefore conceivable that dP2X receptors act as the calcium release channels from this store. Hence, although dP2X proteins do not represent the cell surface receptors directly activated by extracellular ATP/ADP, they may play a role in subsequent downstream signaling events by facilitating release of calcium from intracellular stores.

The generation of a quintuple *p2x* null strain also allowed us to directly assess the importance of dP2X receptors in osmoregulation. Previous studies on *p2xA* null *Dictyostelium* reported that these cells were incapable of regulating their cell volume in water (5). It was therefore unexpected that the five single *p2x* null strains generated in this study showed no obvious osmoregulatory defects (supplemental Fig. S2). Even the complete absence of all five dP2X proteins in the quintuple *p2x* null strain did not prevent cells from undergoing an osmoregulatory decrease in cell volume after initially swelling in water. These cells, however, did show a delay of ~15 min compared with wild type in the onset of a regulatory decrease in volume, but the rate of the subsequent decrease in volume was very similar to that of the wild-type cells (Fig. 8). This is in marked contrast to the behavior of the *p2xA* null cells described by Fountain and co-workers (5), which showed no regulatory decrease in volume and a ~50% increase in size after 60 min in water. Similar to this previous study we also found copper to inhibit the osmoregulatory response in wild-type cells (Fig. 8). We confirm that copper inhibits dP2XA channel function (Fig. 3). However, the effects of copper on osmoregulation cannot be by inhibition of dP2XA as had been previously claimed (5), because copper also inhibits the quintuple *p2x* null strain, which is devoid of P2X receptors. Our results call into question the importance of dP2X receptor function in osmoregulation. The fact that quintuple *p2x* null cells are able to undergo an osmoregulatory response demonstrates that these receptors are not required. However, the slight delay in the onset of the osmoregulatory response indicates that they may play a minor role.

This study has further highlighted the usefulness of *Dictyostelium* as a model system for purinergic signaling. In addition to elucidation of the novel intracellular roles played by intracellular P2X receptors and structure function studies comparing weakly related archetypal dP2X receptors with their vertebrate counterparts, future studies in this model organism may also yield some surprises, because even in the complete absence of dP2X receptors, a robust purinergic calcium response to extracellular ATP/ADP persists. This, together with the fact that extracellular purinergic signaling is also unaffected in *iplA* and *Gβ* null cells (10), which would be contrary to the involvement of a metabotropic P2Y receptor, suggests that a novel type of purinergic receptor or signaling mechanism exists in this organism.

Acknowledgments—We are grateful to David Traynor for advice regarding knock-out generation and to Paul Fisher for the apoaequorin plasmid.

REFERENCES

1. Burnstock, G., and Verkhratsky, A. (2009) *Acta Physiol.* **195,** 415–447
2. Khakh, B. S., and North, R. A. (2006) *Nature* **442,** 527–532
3. North, R. A. (2002) *Physiol. Rev.* **82,** 1013–1067
4. Agboh, K. C., Webb, T. E., Evans, R. J., and Ennion, S. J. (2004) *J. Biol. Chem.* **279,** 41650–41657
5. Fountain, S. J., Parkinson, K., Young, M. T., Cao, L., Thompson, C. R., and North, R. A. (2007) *Nature* **448,** 200–203
6. Fountain, S. J., Cao, L., Young, M. T., and North, R. A. (2008) *J. Biol. Chem.* **283,** 15122–15126
7. Bavan, S., Straub, V. A., Blaxter, M. L., and Ennion, S. J. (2009) *BMC Evol. Biol.* **9,** 17
8. Eichinger, L., Pachebat, J. A., Glöckner, G., Rajandream, M. A., Sucgang, R., Berriman, M., Song, J., Olsen, R., Szafranski, K., Xu, Q., Tunggal, B., Kummerfeld, S., Madera, M., Konfortov, B. A., Rivero, F., Bankier, A. T., Lehmann, R., Hamlin, N., Davies, R., Gaudet, P., Fey, P., Pilcher, K., Chen, G., Saunders, D., Sodergren, E., Davis, P., Kerhornou, A., Nie, X., Hall, N., Anjard, C., Hemphill, L., Bason, N., Farbrother, P., Desany, B., Just, E., Morio, T., Rost, R., Churcher, C., Cooper, J., Haydock, S., van Driessche, N., Cronin, A., Goodhead, I., Muzny, D., Mourier, T., Pain, A., Lu, M., Harper, D., Lindsay, R., Hauser, H., James, K., Quiles, M., Madan Babu, M., Saito, T., Buchrieser, C., Wardroper, A., Felder, M., Thangavelu, M., Johnson, D., Knights, A., Loulseged, H., Mungall, K., Oliver, K., Price, C., Quail, M. A., Urushihara, H., Hernandez, J., Rabbinowitsch, E., Steffen, D., Sanders, M., Ma, J., Kohara, Y., Sharp, S., Simmonds, M., Spiegler, S., Tivey, A., Sugano, S., White, B., Walker, D., Woodward, J., Winckler, T., Tanaka, Y., Shaulsky, G., Schleicher, M., Weinstock, G., Rosenthal, A., Cox, E. C., Chisholm, R. L., Gibbs, R., Loomis, W. F., Platzer, M., Kay, R. R., Williams, J., Dear, P. H., Noegel, A. A., Barrell, B., and Kuspa, A. (2005) *Nature* **435,** 43–57
9. Kreppel, L., Fey, P., Gaudet, P., Just, E., Kibbe, W. A., Chisholm, R. L., and Kimmel, A. R. (2004) *Nucleic Acids Res.* **32,** D332–333
10. Ludlow, M. J., Traynor, D., Fisher, P. R., and Ennion, S. J. (2008) *Cell Calcium* **44,** 567–579
11. Bo, X., Jiang, L. H., Wilson, H. L., Kim, M., Burnstock, G., Surprenant, A., and North, R. A. (2003) *Mol. Pharmacol.* **63,** 1407–1416
12. Barish, M. E. (1983) *J. Physiol.* **342,** 309–325
13. Nebl, T., and Fisher, P. R. (1997) *J. Cell Sci.* **110,** 2845–2853
14. Clarke, M., Köhler, J., Arana, Q., Liu, T., Heuser, J., and Gerisch, G. (2002) *J. Cell Sci.* **115,** 2893–2905
15. Faix, J., Kreppel, L., Shaulsky, G., Schleicher, M., and Kimmel, A. R. (2004) *Nucleic Acids Res.* **32,** e143
16. Manstein, D. J., Schuster, H. P., Morandini, P., and Hunt, D. M. (1995) *Gene* **162,** 129–134
17. Cohen, S. M., Knecht, D., Lodish, H. F., and Loomis, W. F. (1986) *EMBO J.* **5,** 3361–3366
18. Vervoort, E. B., van Ravestein, A., van Peij, N. N., Heikoop, J. C., van Haastert, P. J., Verheijden, G. F., and Linskens, M. H. (2000) *Nucleic Acids*

Res. **28,** 2069–2074
19. Fischer, M., Haase, I., Simmeth, E., Gerisch, G., and Müller-Taubenberger, A. (2004) *FEBS Lett.* **577,** 227–232
20. Khakh, B. S., Proctor, W. R., Dunwiddie, T. V., Labarca, C., and Lester, H. A. (1999) *J. Neurosci.* **19,** 7289–7299
21. Priel, A., and Silberberg, S. D. (2004) *J. Gen. Physiol.* **123,** 281–293
22. Evans, R. J., Lewis, C., Virginio, C., Lundstrom, K., Buell, G., Surprenant, A., and North, R. A. (1996) *J. Physiol.* **497,** 413–422
23. Schlatterer, C., and Schaloske, R. (1996) *Biochem. J.* **313,** 661–667
24. Kawate, T., Michel, J. C., Birdsong, W. T., and Gouaux, E. (2009) *Nature* **460,** 592–598
25. Marquez-Klaka, B., Rettinger, J., Bhargava, Y., Eisele, T., and Nicke, A. (2007) *J. Neurosci.* **27,** 1456–1466
26. Ennion, S., Hagan, S., and Evans, R. J. (2000) *J. Biol. Chem.* **275,** 29361–29367
27. Roberts, J. A., Digby, H. R., Kara, M., Ajouz, S., Sutcliffe, M. J., and Evans, R. J. (2008) *J. Biol. Chem.* **283,** 20126–20136
28. Riedel, T., Schmalzing, G., and Markwardt, F. (2007) *Biophys. J.* **93,** 846–858
29. Ruppelt, A., Ma, W., Borchardt, K., Silberberg, S. D., and Soto, F. (2001) *J. Neurochem.* **77,** 1256–1265
30. Moniakis, J., Coukell, M. B., and Forer, A. (1995) *J. Biol. Chem.* **270,** 28276–28281
31. Kirsten, J. H., Xiong, Y., Davis, C. T., and Singleton, C. K. (2008) *BMC Cell Biol.* **9,** 71
32. Lewis, C., Neidhart, S., Holy, C., North, R. A., Buell, G., and Surprenant, A. (1995) *Nature* **377,** 432–435
33. Torres, G. E., Egan, T. M., and Voigt, M. M. (1999) *J. Biol. Chem.* **274,** 6653–6659
34. Striedinger, K., Meda, P., and Scemes, E. (2007) *Glia* **55,** 652–662
35. Wen, Y., Starvrou, I., Bersuker, K., Brady, R. J., De Lozanne, A., and O'Halloran, T. J. (2009) *Mol. Biol. Cell* **20,** 4278–4288
36. Qiu, F., and Dahl, G. (2009) *Am. J. Physiol. Cell Physiol.* **296,** C250–255
37. Kuehnel, M. P., Rybin, V., Anand, P. K., Anes, E., and Griffiths, G. (2009) *J. Cell Sci.* **122,** 499–504
38. Kuehnel, M. P., Reiss, M., Anand, P. K., Treede, I., Holzer, D., Hoffmann, E., Klapperstueck, M., Steinberg, T. H., Markwardt, F., and Griffiths, G. (2009) *J. Cell Sci.* **122,** 505–512
39. Malchow, D., Lusche, D. F., Schlatterer, C., De Lozanne, A., and Müller-Taubenberger, A. (2006) *BMC Dev. Biol.* **6,** 31